J|A|C|S ARTICLES

Published on Web 02/05/2010

Photoelectrochemical Processes in Polymer-Tethered CdSe Nanocrystals

R. Clayton Shallcross, Gemma D. D'Ambruoso, Jeffrey Pyun, and Neal R. Armstrong*

Department of Chemistry, University of Arizona, Tucson, Arizona 85721

Received September 13, 2009; E-mail: nra@email.arizona.edu

Abstract: We demonstrate the electrochemical capture of CdSe semiconductor nanocrystals (NCs), with thiophene-terminated carboxylic acid capping ligands, at the surfaces of electrodeposited poly(thiophene) films (i) poly((diethyl)propylenedixoythiophene), $P(Et)_2$ProDOT; (ii) poly(propylenedioxythiophene), PProDOT; and (iii) poly(ethylenedioxythiophene), PEDOT, coupled with the exploration of their photoelectrochemical properties. Host polymer films were created using a kinetically controlled electrodeposition protocol on activated indium−tin oxide electrodes (ITO), producing conformal films that facilitate high rates of electron transfer. ProDOT-terminated, ligand-capped CdSe-NCs were captured at the outer surface of the host polymer films using a unique pulse-potential step electrodeposition protocol, providing for nearly close-packed monolayers of the NCs at the host polymer/solution interface. These polymer-confined CdSe NCs were used as sensitizers in the photoelectrochemical reduction of methyl viologen (MV^{+2}). High internal quantum efficiencies (IQEs) are estimated for photoelectrochemical sensitized MV^{+2} reduction using CdSe NCs ranging from 3.1 to 7.0 nm diameters. Cathodic photocurrent at high MV^{+2} concentrations are limited by the rate of hole-capture by the host polymer from photoexcited NCs. The rate of this hole-capture process is determined by (a) the onset potential for reductive dedoping of the host polymer film; (b) the concentration ratio of neutral to oxidized forms of the host polymer ([*P*(n)]/[*P*(ox)]); and (c) the NC diameter, which controls its valence band energy, E_{VB}. These relationships are consistent with control of photoinduced electron transfer by Marcus-like excess free energy relationships. Our electrochemical assembly methods provide an enabling route to the capture of functional NCs in conducting polymer hosts in both photoelectrochemical and photovoltaic energy conversion systems.

Introduction

Semiconducting nanocrystals (NCs) or quantum dots (QDs) are seeing increasing application in photoelectrochemical (PEC) cells,[1−6] and hybrid photovoltaic (PV) cells,[7−11] for production of both solar fuels and electricity. Their unique physical properties and well established synthetic protocols provide for precise control of their size, shape, and their frontier orbital energies [HOMO/LUMO and conduction band (E_{CB}) and valence band (E_{VB}) energies].[12−17] This tunability is used to manipulate the spectral region over which the NCs absorb and emit radiation,[15,18] and rates of photoinduced electron transfer,[19,20] where the NC is used as either a sensitizer to another semiconductor or polymer host, or as a photoelectrocatalyst. Utilization of semiconductor NCs as the active light-absorbing component in either PEC or PV cells necessitates intimate physical and electrical contact of the NC with a material (or solution), where energy level alignment affords fast photoinduced charge separation (i.e., type-II heterojunction).[7,20] Appropriately ligand-capped NCs can facilitate the formation of

(1) Kamat, P. V. *J. Phys. Chem. C* **2008**, *112*, 18737–18753.
(2) Kamat, P. V. *J. Phys. Chem. C* **2007**, *111*, 2834–2860.
(3) Shallcross, R. C.; D'Ambruoso, G. D.; Korth, B. D.; Hall, H. K.; Zheng, Z. P.; Pyun, J.; Armstrong, N. R. *J. Am. Chem. Soc.* **2007**, *129*, 11310–11311.
(4) Sheeney-Haj-Khia, L.; Basnar, B.; Willner, I. *Angew. Chem., Int. Ed.* **2005**, *44*, 78–83.
(5) Sheeney-Haj-Ichia, L.; Pogorelova, S.; Gofer, Y.; Willner, I. *Adv. Funct. Mater.* **2004**, *14*, 416–424.
(6) Granot, E.; Patolsky, F.; Willner, I. *J. Phys. Chem. B* **2004**, *108*, 5875–5881.
(7) Greenham, N. C.; Peng, X. G.; Alivisatos, A. P. *Phys. Rev. B* **1996**, *54*, 17628–17637.
(8) Wang, P.; Abrusci, A.; Wong, H. M. P.; Svensson, M.; Andersson, M. R.; Greenham, N. C. *Nano Lett.* **2006**, *6*, 1789–1793.
(9) Sun, B. Q.; Greenham, N. C. *Phys. Chem. Chem. Phys.* **2006**, *8*, 3557–3560.
(10) Milliron, D. J.; Gur, I.; Alivisatos, A. P. *MRS Bull.* **2005**, *30*, 41–44.
(11) Huynh, W. U.; Dittmer, J. J.; Alivisatos, A. P. *Science* **2002**, *295*, 2425–2427.
(12) Alivisatos, A. P. *J. Phys. Chem.* **1996**, *100*, 13226–13239.
(13) Murray, C. B.; Norris, D. J.; Bawendi, M. G. *J. Am. Chem. Soc.* **1993**, *115*, 8706–8715.
(14) Peng, X. G.; Thessing, J. *Semicond. Nanocryst. Silicate Nanopart.* **2005**, *118*, 79–119.
(15) Qu, L. H.; Peng, X. G. *J. Am. Chem. Soc.* **2002**, *124*, 2049–2055.
(16) Wang, C. J.; Shim, M.; Guyot-Sionnest, P. *Science* **2001**, *291*, 2390–2392.
(17) Meulenberg, R. W.; Lee, J. R. I.; Wolcott, A.; Zhang, J. Z.; Terminello, L. J.; van Buuren, T. *ACS Nano* **2009**, *3*, 325–330.
(18) Yu, W. W.; Qu, L.; Guo, W.; Peng, X. *Chem. Mater.* **2003**, *15*, 2854–2860.
(19) Kongkanand, A.; Tvrdy, K.; Takechi, K.; Kuno, M.; Kamat, P. V. *J. Am. Chem. Soc.* **2008**, *130*, 4007–4015.
(20) Robel, I.; Kuno, M.; Kamat, P. V. *J. Am. Chem. Soc.* **2007**, *129*, 4136–4137.

10.1021/ja907782f

such interfaces, providing for fast charge transfer, enhanced chemical stability, and solution processability.[3,21−23]

A wealth of synthetic techniques are available for producing well-defined sizes and morphologies (e.g., spheres,[15] rods,[24] tetrapods,[24,25] and hyperbranched structures),[26] for CdSe NCs and related II−VI semiconductor NCs, which have now been extensively studied in energy conversion platforms.[1,2] For example, CdSe NCs have been employed as photosensitizers in thin film PEC cells,[3,27,28] quantum-dot-sensitized solar cells (NC-SSCs),[19,29−31] all-inorganic nanocrystal PVs,[32−34] and hybrid nanocrystal/polymer bulk heterojunction PVs,[7,9,35,36] where the NCs not only act as the primary light absorber, but also as the electron transport material. Ligand-capped CdSe NCs have been assembled into photoactive thin films by a variety of methods including spin coating (usually as a blend with an electron donating/hole transporting semiconducting polymer),[37] chemisorption,[5,38,39] electrophoretic deposition,[27,40] and electrochemical cross-linking methods.[3,6,28] Optimized architectures provide for vectorial electron transfer and transport (i.e., a well-defined heterojunction is formed between the nanocrystal and electron donating and electron accepting materials), where back reactions may be slowed by spatially separating free carriers (in a PV cell) or the products of redox reactions (in a PEC cell).[41,42] The need for asymmetric photoelectrochemical and photovoltaic energy conversion systems, involving II−VI semiconductor NCs, has been recognized for some time, but has not been easily achieved with the nanocrystalline forms of these materials.

Figure 1 illustrates our bottom-up electrochemical assembly protocol and photoelectrochemical reactions of nanocomposite polymer films composed of electron-rich thiophene polymers covalently linked to functional CdSe nanocrystals, which are, in turn, "wired" to the substrate transparent electrode [e.g., indium tin oxide (ITO) electrodes].[3] Electrochemical cross-linking methods allow for the tethering of monolayers of CdSe NCs at the polymer film/solution interface. This architecture creates an asymmetric photoactive layer that is an essential component for energy conversion systems which must exhibit vectorial charge separation at the interface between a host polymer, a photosensitizing NC assembly, and solution electron acceptors such as methyl viologen (MV^{+2}), or another condensed phase electron transport layer.

We show here that the net photocurrent for the NC-sensitized reduction of MV^{+2} by the host polymer appears to be limited by the excess free energy available for electron transfer from the polymer host to the photoexcited NC (hole-capture by the polymer). This excess free energy is controlled by the frontier orbital energies of the polymer host, the concentration ratio of neutral to oxidized forms of the polymer host ([*P*(n)]/[*P*(ox)]), and the valence band energy (E_{VB}) for the CdSe NC. We focus here on a series of thiophene-based host polymers: (i) poly-((diethyl)propylenedixoythiophene), $P(Et)_2$ProDOT; (ii) poly(propylenedioxythiophene), PProDOT; and (iii) poly(ethylenedioxythiophene), PEDOT, and CdSe NCs varying from 3.3 to 7.0 nm diameter. Small structural variations in these polymers provides for a systematic adjustment in their electronic properties and, therefore, the rates of hole-capture from the photoexcited NC. Hole-capture rates are also dependent on the size of the CdSe NC (ranging from 3.3 to 7.0 nm), which controls E_{VB} of the NC,[43−45] and, therefore, the excess free energy in the hole-capture process. Marcus-like excess free energy relationships[46] appear to control rates of hole-capture by the host polymer and govern the overall efficiency of the photoinduced electron transfer processes in these hybrid NC/polymer thin films, which may find application in both photoelectrocatalytic and photovoltaic energy conversion technologies.

Results and Discussion

Electrochemical Deposition and Morphology of CdSe NC-Sensitized Thiophene Polymer Films. Figure 1 displays the general methodology for the creation of CdSe NC-sensitized poly(thiophene) films tethered to ITO substrates.[3,47] Experimental details are fully described in Supporting Information. Compositional asymmetry is introduced into this assembly by electrodeposition of the host polymer first, followed by electrochemical capture of the thiophene-capped NCs at the polymer/solution interface. Polymer host films were selected with frontier orbital energy levels and redox activity which would facilitate creation of a "hole-selective" contact, provided that dense electrodeposited films could be formed.[48−51]

Solvent-cleaned ITO electrodes were activated by a combination of air plasma cleaning followed by removal of the top ca.

(21) Liu, J.; Tanaka, T.; Sivula, K.; Alivisatos, A. P.; Frechet, J. M. J. *J. Am. Chem. Soc.* **2004**, *126*, 6550–6551.
(22) Milliron, D. J.; Alivisatos, A. P.; Pitois, C.; Edder, C.; Frechet, J. M. J. *Adv. Mater.* **2003**, *15*, 58–61.
(23) Skaff, H.; Sill, K.; Emrick, T. *J. Am. Chem. Soc.* **2004**, *126*, 11322–11325.
(24) Peng, Z. A.; Peng, X. G. *J. Am. Chem. Soc.* **2002**, *124*, 3343–3353.
(25) Manna, L.; Scher, E. C.; Alivisatos, A. P. *J. Am. Chem. Soc.* **2000**, *122*, 12700–12706.
(26) Kanaras, A. G.; Sonnichsen, C.; Liu, H. T.; Alivisatos, A. P. *Nano Lett.* **2005**, *5*, 2164–2167.
(27) Farrow, B.; Kamat, P. V. *J. Am. Chem. Soc.* **2009**, *131*, 11124–11131.
(28) Yildiz, H. B.; Tel-Vered, R.; Willner, I. *Adv. Funct. Mater.* **2008**, *18*, 3497–3505.
(29) Robel, I.; Subramanian, V.; Kuno, M.; Kamat, P. V. *J. Am. Chem. Soc.* **2006**, *128*, 2385–2393.
(30) Lee, H. J.; Yum, J.-H.; Leventis, H. C.; Zakeeruddin, S. M.; Haque, S. A.; Chen, P.; Seok, S. I.; Grätzel, M.; Nazeeruddin, M. K. *J. Phys. Chem. C* **2008**, *112*, 11600–11608.
(31) Hodes, G. *J. Phys. Chem. C* **2008**, *112*, 17778–17787.
(32) Ma, W.; Luther, J. M.; Zheng, H. M.; Wu, Y.; Alivisatos, A. P. *Nano Lett.* **2009**, *9*, 1699–1703.
(33) Gur, I.; Fromer, N. A.; Geier, M. L.; Alivisatos, A. P. *Science* **2005**, *310*, 462–465.
(34) Luther, J. M.; Law, M.; Beard, M. C.; Song, Q.; Reese, M. O.; Ellingson, R. J.; Nozik, A. J. *Nano Lett.* **2008**, *8*, 3488–3492.
(35) Sun, B. Q.; Snaith, H. J.; Dhoot, A. S.; Westenhoff, S.; Greenham, N. C. *J. Appl. Phys.* **2005**, *97*, 014914.
(36) Gur, I.; Fromer, N. A.; Chen, C. P.; Kanaras, A. G.; Alivisatos, A. P. *Nano Lett.* **2007**, *7*, 409–414.
(37) Krebs, F. C. *Sol. Energy Mater. Sol. Cells* **2009**, *93*, 394–412.
(38) Yildiz, H. B.; Tel-Vered, R.; Willner, I. *Angew. Chem., Int. Ed.* **2008**, *47*, 6629–6633.
(39) Sheeney-Haj-Ichia, L.; Wasserman, J.; Willner, I. *Adv. Mater.* **2002**, *14*, 1323–1326.
(40) Brown, P.; Kamat, P. V. *J. Am. Chem. Soc.* **2008**, *130*, 8890–8891.
(41) Nozik, A. J.; Memming, R. *J. Phys. Chem.* **1996**, *100*, 13061–13078.
(42) Meissner, D.; Memming, R.; Kastening, B. *Chem. Phys. Lett.* **1983**, *96*, 34–37.
(43) Smith, A. M.; Nie, S. *Acc. Chem. Res.* **2010**, in press.
(44) Brus, L. E. *J. Chem. Phys.* **1983**, *79*, 5566–5571.
(45) Munro, A. M.; Zacher, B.; Armstrong, N. R. *ACS Appl. Mater. Interfaces*, submitted.
(46) Marcus, R. A.; Sutin, N. *Biochim. Biophys. Acta* **1985**, *811*, 265–322.
(47) Shallcross, R. C. Ph.D. Dissertation, University of Arizona, 2009.
(48) Marrikar, F. S.; Brumbach, M.; Evans, D.; Lebron-Paler, A.; Pemberton, J.; Wysocki, R.; Armstrong, N. *Langmuir* **2006**, *23*, 1530–1542.
(49) Ratcliff, E. L.; Jenkins, J. L.; Nebesny, K.; Armstrong, N. R. *Chem. Mater.* **2008**, *20*, 5796–5806.
(50) Armstrong, N. R.; Veneman, P. A.; Ratcliff, E.; Placencia, D.; Brumbach, M. *Acc. Chem. Res.* **2009**, *42*, 1748.
(51) Steim, R.; Choulis, S. A.; Schilinsky, P.; Brabec, C. J. *Appl. Phys. Lett.* **2008**, *92*, 3.

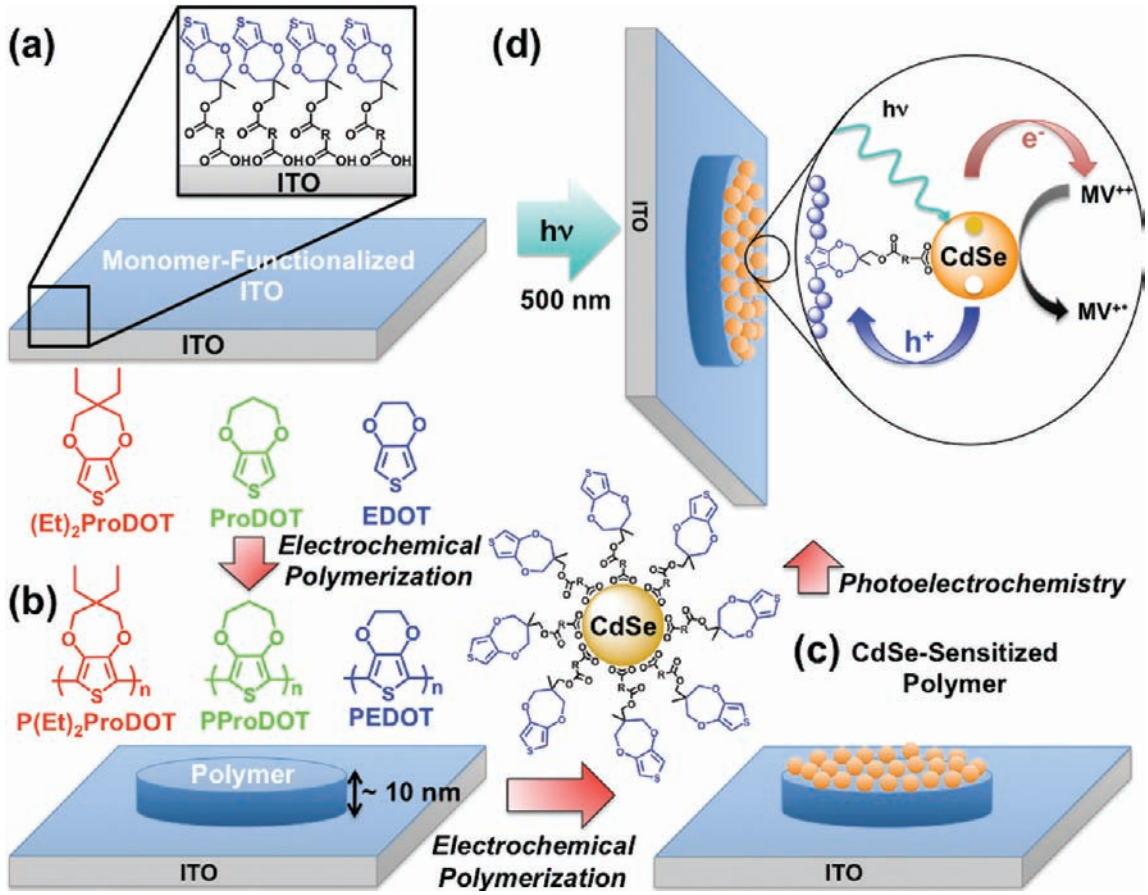

Figure 1. Illustration of the bottom-up electrochemical preparation of CdSe NC-sensitized poly(thiophene) films, "wired" to indium tin oxide (ITO) substrates. This approach ensures placement of the NC at the polymer/solution interface, providing for vectorial electron transport when the redox state of the polymer is optimized: (a, b) Electrochemical polymerization of electron-rich thiophene monomers onto ProDOT-CA-modified ITO substrates affords conformal poly(thiophene) films, optimized to provide enhanced rates of charge transfer to the hole collection electrode [R = $(CH_2)_8$ on the ProDOT-CA molecule]. (c) Electrochemical capture of ProDOT-CA-functionalized CdSe NCs at the polymer/solution interface, using a pulsed-potential step electrodeposition protocol, creates a photoelectrochemically active thin film. (d) Photoexcitation at 500 ± 5 nm of these CdSe NC-sensitized polymer films in the presence of an electron acceptor (methyl viologen, MV^{+2}) provides for efficient generation of cathodic photocurrents, limited by the rate of hole capture by the host polymer (electron transfer to the photooxidized NC), which in turn is limited by the offsets between the frontier orbital energies for the partially doped polymer, and the valence band energy (E_{VB}) of the NC.

5−10 nm of the ITO surface using an HI acid etch,[52] and immediate modification by the chemisorption of a monolayer of the electroactive carboxylic acid thiophene-terminated monomer, ProDOT-CA.[3] This combination of surface treatments removes contaminate and modifies the ITO surface with an electroactive monomer, which enhances rates of electron transfer to solution probe molecules for both bare and PEDOT-coated ITO electrodes.[48,52–54] Thiophene-monomer functionalized ITO surfaces also lower the overpotential associated with oxidative electrodepositon of conducting polymer species, corresponding to increased rates of nucleation and polymerization.[49]

$P(Et)_2$ProDOT, PProDOT, and PEDOT polymer films were electrodeposited from 10 mM monomer solutions (0.1 M $TBAPF_6$ in acetonitrile) at constant potentials (1.0, 0.95, and 0.90 V vs Ag/Ag^+, respectively) that ensured slow rates of deposition (i.e., potential regions were selected where electron transfer was kinetically controlled).[3,48] Ultrathin (ca. 10 nm) polymer films resulted from deposition of a total oxidative charge of 2 mC/cm^2. Conformal polymer films were formed that facilitate high rates of electron transfer between the modified ITO electrode and solution probe molecules such as dimethylferrocene.[48]

The morphology of the as-deposited 3,4-dioxy-substituted polymer films on ProDOT-CA functionalized ITO was characterized by field emission scanning electron microscopy (FE-SEM, Figure 2a−c). These electrodeposited polymer films were ca. 10 nm in thickness, and the images reflect the topography of the underlying ITO substrate (Figure 2a inset), showing the typical subgrain structure of this oxide substrate.[52,55,56] PProDOT polymer films (Figure 2b) display areas of increased nanoscale texturing, while $P(Et)_2$ProDOT and PEDOT films (Figure 2a,c, respectively) showed no significant texturing. Electrochemically deposited poly(3,4-alkylenedioxythiophene) derivatives have shown similar differences in film morphology,

(52) Brumbach, M.; Veneman, P. A.; Marrikar, F. S.; Schulmeyer, T.; Simmonds, A.; Xia, W.; Lee, P.; Armstrong, N. R. *Langmuir* **2007**, *23*, 11089–11099.
(53) Carter, C.; Brumbach, M.; Donley, C.; Hreha, R. D.; Marder, S. R.; Domercq, B.; Yoo, S.; Kippelen, B.; Armstrong, N. R. *J. Phys. Chem. B* **2006**, *110*, 25191–25202.
(54) Armstrong, N. R.; Carter, C.; Donley, C.; Simmonds, A.; Lee, P.; Brumbach, M.; Kippelen, B.; Domercq, B.; Yoo, S. *Thin Solid Films* **2003**, *445*, 342–352.
(55) Popovich, N. D.; Wong, S. S.; Ufer, S.; Sakhrani, V.; Paine, D. *J. Electrochem. Soc.* **2003**, *150*, H255–H259.
(56) Popovich, N. D.; Wong, S. S.; Yen, B. K. H.; Yeom, H. Y.; Paine, D. C. *Anal. Chem.* **2002**, *74*, 3127–3133.

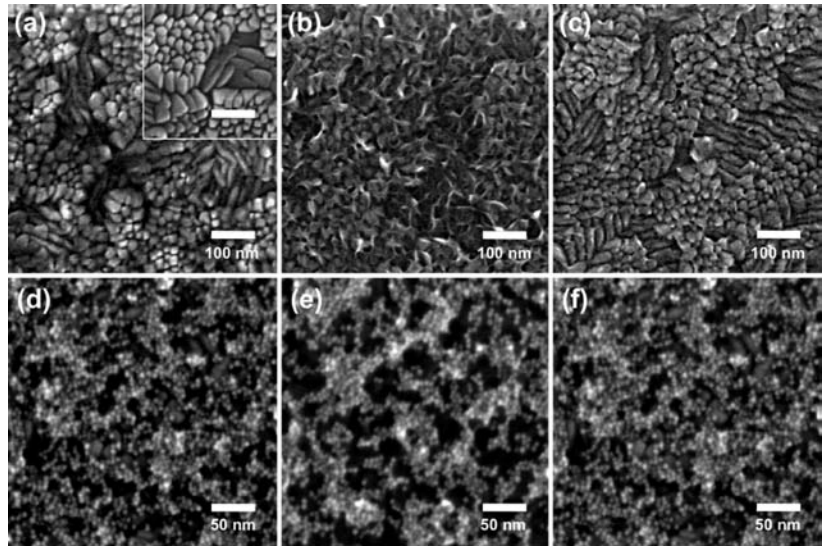

Figure 2. Plane-view FE-SEM images of poly(thiophenes) (a, b, and c) and CdSe NC (5 nm)-sensitized poly(thiophene) films (d, e, and f), prepared by electrodepositon onto ProDOT-CA-functionalized ITO substrates. Images a, b, and d correspond to $P(Et)_2$ProDOT, PProDOT, and PEDOT polymer films (2 mC cm^{-2}, ca. 10 nm in thickness), respectively. The inset in part a represents a bare ITO substrate (scale bar = 100 nm). Images d, e, and f correspond to $P(Et)_2$ProDOT, PProDOT, and PEDOT polymer films with electrochemically captured ProDOT-CA-functionlized CdSe NCs (5.0 nm), respectively, at close to monolayer coverages.

which is a product of differences in both the chemical structure of the monomer and/or the applied potential during their electrochemical polymerization.[57]

ProDOT-CA-functionalized CdSe NCs (5.0 nm, 10 μM) were next captured at the surface of each host polymer film using a pulsed potential step electrodeposition protocol, adapted from methodologies introduced by Schuhmann et al. for capture of enzymes in electrodeposited polymer films.[49,58,59] The electrode potential is first stepped to +1.10 V (0.1 s), where poly(thiophene) electrodeposition is kinetically controlled, followed by a longer rest pulse at 0.40 V for 1.0 s, where no polymerization or cross-linking of CdSe NCs takes place. The polymerization pulse takes place at potentials known to oxidize and cross-link the ProDOT functional groups on the CdSe NC to the surface of the host polymer film and/or with nearby NCs, rendering the ligand-capped NC insoluble.[60,61] Fifteen deposition/rest pulses were applied to produce the highest possible NC coverage, while retaining both the chemical and physical integrity, and photoelectrochemical activity, of the polymer-bound NCs.

This multipotential step method was chosen over more traditional electrodeposition methods, considering the relatively large size and small diffusion coefficients of ligand-capped nanocrystals (i.e., CdSe NC diffusion coefficients of ca. 10^{-7} cm^2/s have been reported).[62,63] Rest pulse lengths were chosen which were at least 10× the deposition pulse length to ensure "refilling" of the depletion layer near the electrode surface, before electrodeposition was resumed.[59] Other electrochemical polymerization strategies were evaluated, including the use of more than 15 deposition/rest pulses; however, this approach provided the best control over NC coverage and subsequent photoelectrochemical viability.[47]

Figure 2d−f displays representative FE-SEM images of 5 nm CdSe NC-decorated polymer films. Individual particles and more often clusters of NCs are easily resolved, with occasional regions of bare polymer film. These NC-decorated polymer films were quite robust; sonication in neat THF (a good solvent for the ProDOT-CA-functionalized NCs)[47] did not produce a noticeable change in NC surface coverage.

NC loading (surface coverage) on each polymer surface was estimated by counting individual and clustered NCs for at least four randomly selected images like those shown in Figure 2d−f. These measurements were then compared to the expected coverage for a hexagonally closest packed (hcp) monolayer of ligand-capped CdSe NCs in order to estimate fractional surface coverages, reported below as "equivalent monolayers" or EMLs. NC coverage on each polymer appeared to be similar with values of 64 ± 7, 59 ± 6, 63 ± 5% EML for $P(Et)_2$ProDoT, PProDOT, and PEDOT, respectively (see the Supporting Information Figure S1 for the detailed methodology of estimating relative coverages).

NC coverages were also estimated using absorbance spectra of these thin films; however, the absorbance due to monolayer NC films (ca. 0.001 au) was difficult to resolve above the background absorbance from the polymer, and coverages estimated from such data were not more reliable than coverages estimated from the FE-SEM images. These coverages, along with extinction spectra of the nanocrystals, were used to compare the normalized photoelectrochemical efficiency, i.e., the internal quantum yield (IQE) of charge collection in these systems (see below).

Voltammetric Characterization of Poly(thiophene) and CdSe NC-Sensitized Poly(thiophene) Films. Figure 3 shows the voltammograms (100 mV/s) of $P(Et)_2$ProDoT, PProDOT, and

(57) Groenendaal, L.; Zotti, G.; Aubert, P. H.; Waybright, S. M.; Reynolds, J. R. *Adv. Mater.* **2003**, *15*, 855–879.
(58) Ratcliff, E. L., Lee, P. A., Armstrong, N. R. *J. Mater. Chem.*, in press.
(59) Schuhmann, W.; Kranz, C.; Wohlschlager, H.; Strohmeier, J. *Biosens. Bioelectron.* **1997**, *12*, 1157–1167.
(60) Zotti, G.; Zecchin, S.; Vercelli, B.; Berlin, A.; Grimoldi, S.; Groenendaal, L.; Bertoncello, R.; Natali, M. *Chem. Mater.* **2005**, *17*, 3681–3694.
(61) Heinze, J.; Rasche, A.; Pagels, M.; Geschke, B. *J. Phys. Chem. B* **2007**, *111*, 989–997.
(62) Pons, T.; Uyeda, H. T.; Medintz, I. L.; Mattoussi, H. *J. Phys. Chem. B* **2006**, *110*, 20308–20316.
(63) Bard, A. J.; Faulkner, L. R. *Electrochemical Methods Fundamentals and Applications*, 2nd ed.; John Wiley & Sons, Inc.: New York, 2001.

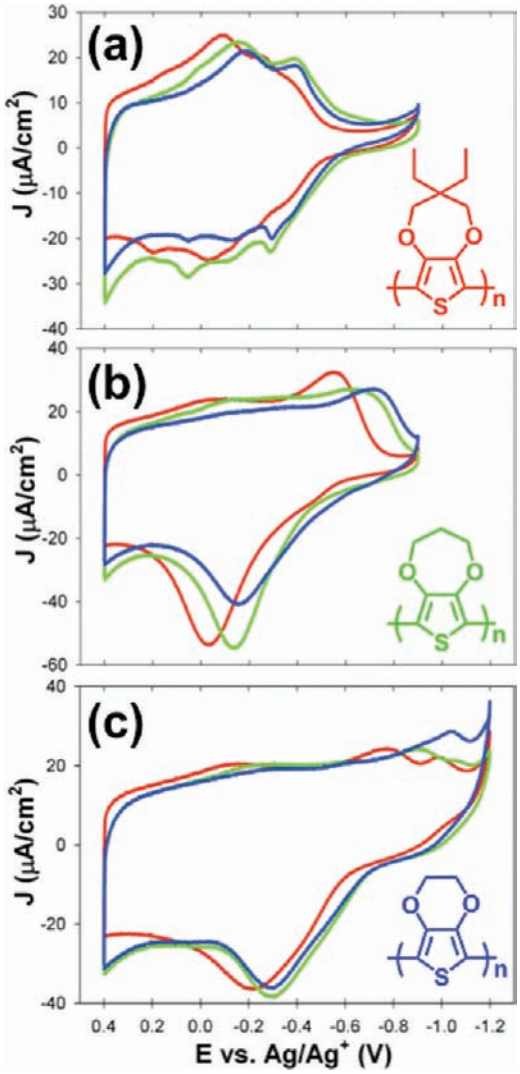

Figure 3. Cyclic voltammograms (100 mV/s; 2nd scans) of 2 mC cm^{-2} (ca. 10 nm thickness) (a) $P(Et)_2$ProDOT, (b) PProDOT, and (c) PEDOT polymer films synthesized by constant potential electropolymerization of monomers (10 mM; in 0.1 M $TBAPF_6$ in acetonitrile) on ProDOT-CA-functionalized ITO electrodes at 1.0, 0.95, and 0.90 V, respectively. The red curves correspond to CVs of the polymer in acetonitrile solution (0.1 M $TBAPF_6$). The green and blue curves correspond to CVs of the polymer film in the presence of 5 nm diameter ProDOT-CA-functionalized CdSe NCs [ca. 10 μM; in 0.15 M $TBAPF_6$ in THF/acetonitrile (2/1, v/v)] before and after NC cross-linking, respectively.

PEDOT polymer films (2 mC/cm^2) in acetonitrile solution (red curves) and in THF/acetonitrile solutions containing ProDOT-CA-functionalized CdSe NCs (5.0 nm), before (green curves) and after (blue curves) capturing the CdSe NCs at the polymer/solution interface. Scanning the applied potential of the initially neutral (dedoped) polymer film electrode to positive potentials initiates oxidative doping of the polymer backbone; positive charges are compensated by anion insertion.[64] The scan direction is switched in a potential region where the polymer is reversibly oxidized. The shapes of the voltammograms for each polymer are different, which is a product of substitution and structure of the alkyl bridge linker between the oxygen atoms.[57] There is significant hysteresis in the voltammograms between the anodic and cathodic sweeps for PEDOT and PProDOT films, attributable to an overpotential for anion removal from the polymer as the film is returned to the neutral form.[65] $P(Et)_2$ProDOT films produce a more symmetrical oxidation/reduction voltammogram; the diethyl-substitution at the apex of the propylene bridge of $P(Et)_2$ProDOT causes a distortion in the packing of the polymer chains and produces a more disordered electrodeposited polymer film. Reynolds and co-workers have recently demonstrated that the disordered structure of $P(Et)_2$ProDOT polymer films leads to facile ionic transport in this polymer, relative to more ordered PEDOT and PProDOT films.[66]

The polymer films show similar voltammetric responses in acetonitrile and THF/acetonitrile solutions suggesting that no significant structural rearrangements occurred by adding THF as a cosolvent, which is necessary for solvation of the ProDOT-capped CdSe NCs.[47] The addition of THF as a cosolvent negatively shifts both the poly(thiophene) voltammograms ca. 100 mV, and the formal redox potential for the ferrocene/ferricenium (Fc/Fc^+) redox couple used as a reference. The voltammetric responses of these polymer films in THF/acetonitrile before (green) and after (blue) NC capture were similar; however, polymer redox peak position and magnitude were occasionally slightly altered due to the presence of tethered nanocrystals, which may block electroactive polymer sites and/or perturb ion insertion/deinsertion that accompanies redox cycling of the polymer. Increased NC cross-linking into the polymer host (i.e., utilizing substantially more than 15 polymerization pulses) was accompanied by a decrease in the electroactivity of the underlying polymer film (see Supporting Information Figure S8 for comparison of electroactivities for optimized and higher loadings of CdSe NCs on a PEDOT film).

Photoelectrochemistry of CdSe NC-Sensitized Polymer Films: Effect of Polymer Host. The differences in the molecular structure of these three poly(thiophene) host polymers provide a systematic change in the electronic properties of these polymer hosts, which can be exploited to control rates of hole capture from photoexcited CdSe NCs tethered at the polymer/solution interface. Photoelectrochemical experiments were carried out using bandpass-filtered excitation (500 $\pm$ 5 nm, ca. 2.1 mW/cm^2) of CdSe-NC-sensitized polymer films in the presence of aqueous MV^{+2} solutions/(5 mM).

Photocurrent yields scaled with solution MV^{+2} concentration up to ca. 5 mM, above which no further increases in photocurrent yield were observed. These results suggest that electron capture by MV^{+2} reaches a maximum rate which is not mass transport controlled. It has been suggested that adsorption of MV^{+2} to the surface of colloids such as CdSe NCs occurs at low solution concentrations, providing for rapid quenching of electron transfer events with semiconducting NCs, independent of quencher concentration.[67−70] Kamat and co-workers have shown that electron injection from photoexcited dioctyl sulfosuccinate (AOT)-capped CdSe NCs into MV^{+2} is fast, with NC excited state half-lives of ca. 40 ps in the presence of MV^{+2}.[67] As discussed below, the driving force for electron capture by MV^{+2} from the photoexcited NC is also apparently higher than

(64) Carlberg, C.; Chen, X. W.; Inganas, O. *Solid State Ionics* **1996**, *85*, 73–78.
(65) Bilger, R.; Heinze, J. *Synth. Met.* **1993**, *55*, 1424–1429.
(66) Gaupp, C. L.; Welsh, D. M.; Reynolds, J. R. *Macromol. Rapid Commun.* **2002**, *23*, 885–889.
(67) Harris, C.; Kamat, P. V. *ACS Nano* **2009**, *3*, 682–690.
(68) Graetzel, M.; Frank, A. J. *J. Phys. Chem.* **1982**, *86*, 2964–2967.
(69) Logunov, S.; Green, T.; Marguet, S.; El-Sayed, M. A. *J. Phys. Chem. A* **1998**, *102*, 5652–5658.
(70) Burda, C.; Green, T. C.; Link, S.; El-Sayed, M. A. *J. Phys. Chem. B* **1999**, *103*, 1783–1788.

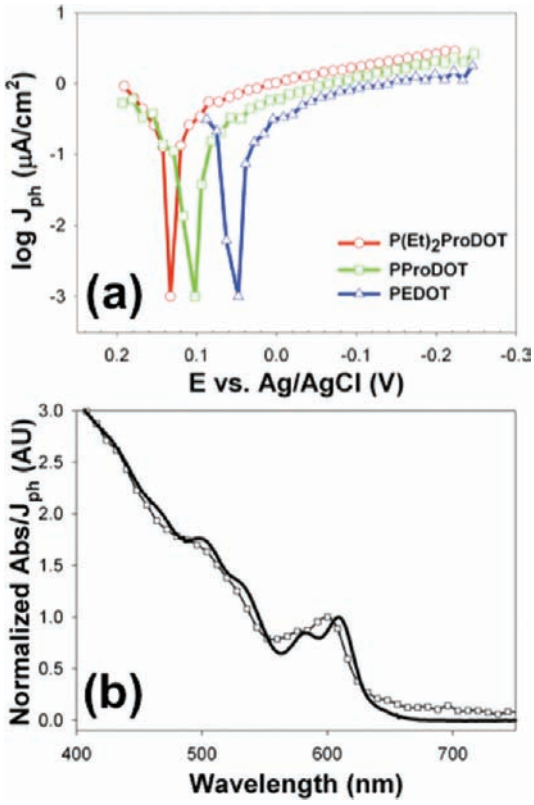

Figure 4. (a) Semilog photocurrent (J_{ph}) vs potential plots for CdSe NC (5 nm)-sensitized P(Et)$_2$ProDOT (red circles/line), PProDOT (green squares/line), and PEDOT (blue triangles/line) polymer films in the presence of MV^{+2} (5 mM in aqueous 0.1 M $LiClO_4$). Excitation was performed with 500 ± 5 nm radiation (2.1 mW cm^{-2}) using a band-pass-filtered Xe arc lamp. (b) The photocurrent action spectrum (−0.15 V; black squares/line) of CdSe NC-sensitized polymer films closely resembles the solution absorption spectra of these same ligand-capped CdSe NCs (black line) suggesting that cathodic photocurrent arises solely from photoexcited CdSe NCs attached to the polymer host.

for hole-capture by the host polymer, and at MV^{+2} concentrations at or above 5 mM, we show that hole capture from the photoexcited CdSe NC by the host polymer is the photocurrent limiting step.

Figure 4a shows representative log (absolute value) of background corrected photocurrent versus potential for CdSe NC (5 nm)-sensitized PEDOT, PProDOT, and P(Et)$_2$ProDOT films. Both reduction (net photosensitized reduction of MV^{+2} by the host polymer) and oxidation photocurrents are observed, becoming equal at "onset" potentials that are unique for each poly(thiophene) host film (see Supporting Information Figure S3 for the dark and illuminated current−voltage behavior). The cathodic photocurrent for each NC-sensitized polymer film increased exponentially with applied potential, starting ca. 50 mV negative of the onset potential. The onset potentials for onset of cathodic photocurrents were well positive of the MV^{+2}/$MV^{+\bullet}$ formal reduction potential (−0.65 V vs Ag/AgCl).[67,68] In a fully rectifying photoelectrochemical closed cycle redox energy conversion system we predict open-circuit photopotentials in a range from 0.7 to 0.8 V for each NC-modified polymer film.

Figure 4b shows a representative photocurrent action spectrum of a CdSe (ca. 5 nm)-P(Et)$_2$ProDOT film at −0.15 V (both PEDOT and PProDOT films provided similar spectra). These action spectra were comparable to the solution absorption spectra for the ligand-capped NCs, demonstrating that the cathodic photocurrent response arises solely from polymer-tethered CdSe NCs. The small blue shift in the action spectra of the CdSe NC-sensitized polymer films, versus their solution absorbance spectra, may be attributable to slight etching of the CdSe NCs during the cross-linking step,[3] which may be a byproduct of direct electrochemical oxidation and/or reactions involving locally generated protons, which are a known byproduct of thiophene monomer coupling reactions.[61] We also explored the photoelectrochemical responses of the host polymer films, in the absence of CdSe NCs. At this potential (i.e., −0.15 V), PEDOT, PProDOT, and P(Et)$_2$ProDOT control films show significantly smaller (or undetectable) photocurrents compared to CdSe NC-sensitized films (see Supporting Information Figure S5 for the photoelectrochemical response of the control polymer films).

Factors Controlling Photoelectrochemical Efficiencies. We show here that photoelectrochemical efficiencies are controlled by a series of coupled chemical and electrochemical processes, whose rates are controlled by applied potential, [*P*(n)]/[*P*(ox)], and the diameter (and valence band energy) of the CdSe NC. Figure 5a shows an energy level diagram (relative to the Ag/AgCl reference electrode) summarizing the processes that contribute to the generation of photocurrents in ITO/donor polymer/CdSe NC/MV^{+2}(aq) heterojunctions, using estimated energy levels corrected to the Ag/AgCl reference electrode in acetonitrile/THF. We show a Fermi level defined by the ITO electrode in equilibrium with the redox couple represented by the neutral form of the polymer host, *P*(n), and the polaronic levels associated with the oxidatively doped form of the polymer host (*P*(ox)); i.e., [*P*(n)]/[*P*(ox)] is controlled by the applied potential at the ITO electrode. The energy level associated the MV^{+2}/$MV^{+\bullet}$ redox couple is shown in this diagram as ca. 0.7 V negative of the ITO/host polymer Fermi level, i.e., at the "onset potential" for net cathodic photocurrent. Energy offsets between E_{CB} for the NC and the MV^{+2}/$MV^{+\bullet}$ redox couple, and E_{VB} for the NC and the host polymer redox potential, designated as $\eta_{c,1}$ and $\eta_{c,2}$, respectively.[1,3,16,19,29,47,67]

The individual electron transfer events and their rates (r) are summarized in eqs 1−3, and the overall sensitized electron (e^-) transfer from the host polymer to (MV^{+2}), accompanied by hole (h^+) capture by the neutral donor polymer, *P*(n) is summarized in eq 4:

$$\mathrm{CdSe} + h\nu \rightarrow \mathrm{CdSe}(e^- + h^+) \quad (1)$$

$$\mathrm{CdSe}(e^- + h^+) + MV^{++} \xrightarrow{r_{c,1}} \mathrm{CdSe}(h^+) + MV^{+\bullet} \quad (2)$$

$$\mathrm{CdSe}(h^+) + P(\mathrm{n}) \xrightarrow{r_{c,2}} \mathrm{CdSe} + P(\mathrm{ox})^{+\bullet} \quad (3)$$

$$MV^{++} + P(\mathrm{n}) + h\nu \xrightarrow{\mathrm{CdSe}} MV^{+\bullet} + P(\mathrm{ox})^{+\bullet} \quad (4)$$

The excited state of the CdSe NC is designated CdSe(e^- + h^+) to represent a state of the NC capable of both electron donation to MV^{+2} and electron capture from the host polymer. Competing energy loss and back reaction processes correspond to (i) radiative and nonradiative decay in the NC (r_r and r_{nr}), (ii) electron transfer from the photoexcited NC to polaronic states in the polymer ($P(ox)^{+\bullet}$) ($r_{a,1}$), and (iii) back electron transfer from the reduced methyl viologen radical cation ($MV^{+\bullet}$) to either the oxidized NC or polaronic states in the polymer

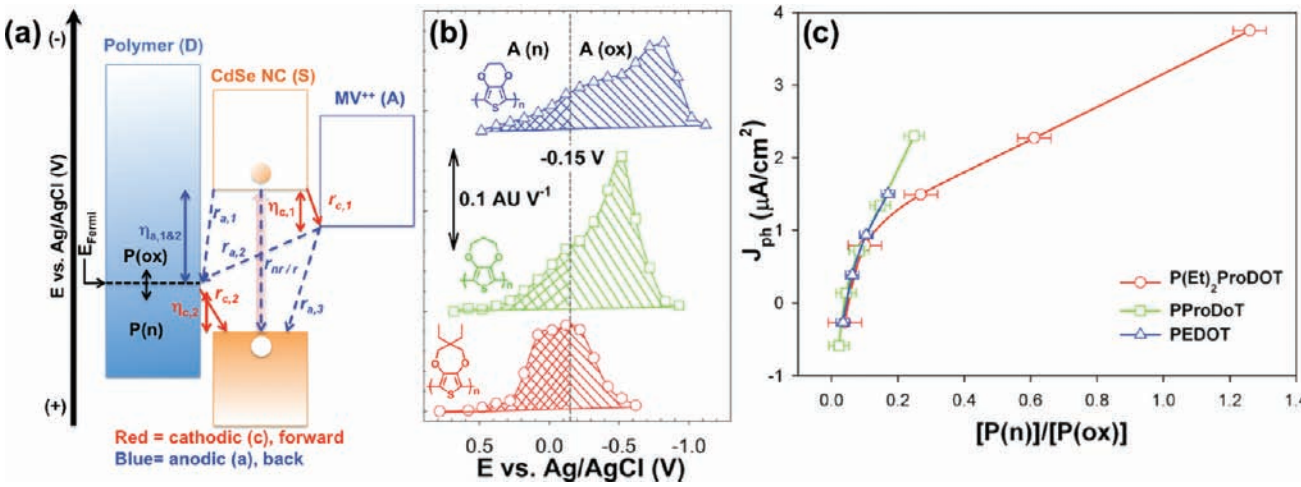

Figure 5. (a) Schematic energy level diagram of the charge transfer processes that determine the magnitude and direction of photocurrent for the donor (D, polymer)−sensitizer (S, CdSe NC)−acceptor (A, MV^{+2}) system. Forward (cathodic, c) electron transfer (ET) is designated with red solid arrows. Back (anodic, a) ET is designated with blue dashed arrows. Reaction rates (r) are denoted with a "c" and "a", respectively. The excess free energy dictating the rate for each process is represented as an overpotential, η. We show the Fermi level of the host polymer, wired to the ITO substrate, as variable, controlling the driving force for both forward and back reactions, controlling both [P(n)]/[P(ox)], and the overpotentials ($\eta_{c,2}$ and $\eta_{a,1\&2}$). For net cathodic photocurrents we assume that photoexcited ET from CdSe NCs to MV^{+2} is fast, and that ET from the host polymer is the rate limiting step. (b) [P(n)]/[P(ox)] in each polymer is determined by the area under the cathodic absorptovoltammogram (plotted as the derivative of the maximum neutral absorbance vs potential; $dA_{max}(n)/dE$). As the ITO/polymer film potential is scanned negatively, [P(n)]/[P(ox)] increases for $P(Et)_2$ProDOT (red circles), PProDOT (green squares), and PEDOT (blue triangles). See Supporting Information Figure S4 for potential dependent difference spectra for each polymer. (c) Plotting the background-corrected J_{ph} as a function of [P(n)]/[P(ox)] demonstrates the similarity in potential-dependent ET around the onset potential for all three polymer hosts, implying that similar processes for each host are responsible for the CdSe NC-photosensitized reduction of MV^{+2}.

($r_{a,2}$ or $r_{a,3}$, respectively). Sensitized reduction of MV^{+2} dominates at potentials negative of the onset potentials shown in Figure 4; back reactions are predicted to dominate at potentials positive of this turn on voltage, along with dark oxidation processes for both the polymer host and the tethered NC. A set of rate equations can be written for these reactions:

$$r_{c,1} = k_{c,1}[MV^{++}][CdSe(e^- + h^+)] \quad (5)$$

$$r_{c,2}(E) = k_{c,2}(E)[P(n)](E)[CdSe(h^+)] \quad (6)$$

$$r_{a,1}(E) = k_{a,1}(E)[P(ox)^{+\bullet}](E)[CdSe(e^- + h^+)] \quad (7)$$

$$r_{a,2}(E) = k_{a,2}(E)[P(ox)^{+\bullet}](E)[MV^{+\bullet}] \quad (8)$$

$$r_{a,3} = k_{a,3}[MV^{+\bullet}][CdSe(h^+)] \quad (9)$$

Potential-dependent rate coefficients are designated as $k_{x,y}(E)$, and those independent of applied potential are designated $k_{x,y}$. We assume that the concentration of MV^{+2}, $MV^{+\bullet}$, CdSe, CdSe*, and CdSe(h^+) are constant (steady state approximation, under constant intensity illumination). We therefore assume that $r_{c,1}$ is constant (eq 5) and independent of applied potential. Equations 6, 7, and 8 can be treated at a fixed potential as pseudo-first-order processes with respect to the neutral (P(n)) or oxidized (P(ox)) forms of the polymer. The forward (cathodic) rate $r_{c,2}$, and the back reaction (anodic) rates $r_{a,1}$, $r_{a,2}$, and $r_{a,3}$ are potential dependent (E) (eqs 6, 7 and 8), inasmuch as applied potential controls the individual concentrations [P(n)], [$P(ox)^{+\bullet}$], their ratio ([P(n)]/[$P(ox)^{+\bullet}$]), and the driving force for electron injection into the polaronic (oxidized) states of the host polymer.

The rate-limiting step, $k_{c,2}$, the photocurrent yield, and the overall photoelectrochemical efficiency are predicted to be exponentially dependent on the excess free energy ($-\Delta G$) in the hole-capture process in a Marcus-like relationship (eq 10):[46]

$$k_{c,2} \propto \exp\left[\frac{-(\Delta G - \lambda_R)^2}{4\lambda_R k_B T}\right] \quad (10)$$

where λ_R is the total reorganization energy for the polymer/ligand-capped NC system, k_B is the Boltzmann constant, and T is the absolute temperature. For potentials ca. 50 mV negative of the onset potential, increasing the driving force (η) for hole capture (i.e., the energetic difference between the Fermi energy of the polymer (the electrochemical potential), and E_{VB} for the NC) produces an exponential increase in the rate of hole capture ($k_{c,2}$) by each of the doped polymers (Figure 4a). Increasing negative potentials also increases [P(n)]/[$P(ox)^{+\bullet}$], which provides a further enhancement of the cathodic photocurrent.

We compare rates of charge transfer between polymer hosts, and between NCs of different diameters, by first considering the factors that affect the internal quantum efficiency (IQE) of cathodic photocurrent yield for each CdSe NC-sensitized polymer film at a single applied voltage, −0.15 V, and a single excitation wavelength (500 nm). IQE is a product of three efficiencies relating to the overall photoelectrochemical process (eq 4):

$$IQE = \phi_{LHE}\phi_{CT,MV^{++}}\phi_{CT,P(n)} \quad (11)$$

ϕ_{LHE} is the efficiency of light absorption (light harvesting efficiency, LHE) by the polymer-tethered CdSe NCs (eq 1), $\phi_{CT,MV^{+2}}$ is the charge transfer (CT) efficiency for reduction of MV^{+2} by photoexcited CdSe NCs (eqs 2 and 5), and $\phi_{CT,P(n)}$ is the efficiency of hole capture from oxidized NCs by neutral forms of the polymer film (eqs 3 and 6).

Both charge transfer efficiency terms in eq 11 may be further expressed as the ratio of rates of the forward (cathodic) photoelectrochemical process, relative to the sum of this forward process and all possible back reactions:

$$\phi_{CT,MV^{++}} = \frac{r_{c,1}}{r_{c,1} + r_{a,1}(E) + r_{a,2}(E) + r_{a,3} + r_r + r_{nr}} \quad (12)$$

$$\phi_{CT,P(n)} = \frac{r_{c,2}(E)}{r_{c,2}(E) + r_{a,3} + r_r + r_{nr}} \quad (13)$$

The assumptions inherent in eq 12 are that $\phi_{CT,MV^{+2}}$ depends only on rates of electron transfer to MV^{+2}, competing with radiative and nonradiative energy loss from CdSe($e^- + h^+$), back electron transfer from CdSe($e^- + h^+$) to the polaronic state (P(ox)), and back electron transfer from $MV^{+\bullet}$ to these same polaronic states. In eq 13 we assume that $\phi_{CT,P(n)}$ depends only on the rates of electron transfer from P(n) to CdSe(h^+) competing with back electron transfer from $MV^{+\bullet}$ to CdSe(h^+) and the radiative and nonradiative energy loss processes associated with CdSe*. The CT efficiencies associated with eqs 12 and 13 are actually coupled complex reactions at potentials near the onset potential for net cathodic photocurrent production. They are enhanced and decoupled with a negative shift in the Fermi potential of the polymer due to a combination of increased driving force for hole capture and larger [P(n)]/[P(ox)] ratios (discussed below).

IQE values at 500 nm (−0.15 V) were estimated by first measuring the incident photon to current generation efficiency (IPCE):

$$\text{IPCE} = \frac{1240 \times J_{ph}(\mu\text{A/cm}^2)}{\lambda(\text{nm}) \times I(\mu\text{W/cm}^2)} \times 100 \quad (14)$$

where λ is the wavelength of excitation (e.g., 500 nm), J_{ph} is the extracted photocurrent, and I is the intensity of the incident radiation (see Supporting Information Figures S6 and S7 for detailed IPCE measurements). Light harvesting efficiency (LHE) of polymer-tethered CdSe NCs was estimated by taking into account their diameter-dependent absorptivity and coverage (estimated from the FE-SEM images shown above). Normalizing the IPCE to LHE provides IQE:

$$\text{IQE} = \frac{\text{IPCE}}{\text{LHE}} \quad (15)$$

IQE is therefore corrected for differences in the coverage and absorptivity of the tethered NCs.

Table 1 summarizes the photoelectrochemical data for 5 nm CdSe NCs electrochemically tethered to P(Et)$_2$ProDOT, PProDOT, and PEDOT host films. The IQE of these films is high, approaching 50% for 5.0 nm NCs (see Supporting Information Figure S1 for details for the estimation of IQE values). In order to more easily compare the efficiency and rate of hole capture by each polymer host at −0.15 V, IQE values were normalized to the highest IQE, obtained for CdSe NCs tethered to P(Et)$_2$ProDOT films. P(Et)$_2$ProDOT host films show the most positive onset potentials for cathodic photocurrent and highest IQE values at −0.15 V, where the driving forces for hole capture are equal for all three polymers. Significant differences in IPCE and IQE are seen for the three NC-modified polymers, which can be understood in the context of the potential-dependent [P(n)]/[P(ox)] ratio in each host polymer.

Spectroelectrochemical Characterization of [*P*(n)]/[*P*(ox)] in Host Polymer Films. Figure 5b shows the derivative of absorbance intensity, determined at a wavelength selective for the neutral form of the polymer, with respect to potential ($\Delta A/\Delta V$, see Supporting Information Figure S7 for full spectroelectrochemical analysis of each polymer film).[71] Figure 5b shows that all three polymers have significant fractions of their neutral forms present at −0.15 V (represented by the integrated area positive of −0.15 V). P(Et)$_2$ProDOT shows the highest fraction of neutral polymer (ca. 50−60%) and the greatest degree of reversibility in the oxidative doping/dedoping process around a narrow potential window (ca. +0.3 to −0.3 V), which ultimately corresponds to a more positive turn on voltage and higher IQE for CdSe NC-sensitized P(Et)$_2$ProDOT films. Figure 5c plots the photocurrent response of each film relative to [P(n)]/[P(ox)] in each polymer film. All NC-modified polymers produce similar photoelectrochemical responses near their onset potentials, since the onset of cathodic photocurrent is dependent on [P(n)]/[P(ox)], and a net cathodic current results only when [P(n)]/[P(ox)] ≥ ca. 0.05, where the rates of MV^{+2} reduction and hole capture by the polymer host exceeds the rates of all other back reactions.

The energetic difference between the Fermi energy of the ITO/polymer electrode and E_{VB} for the NC (i.e., the driving force for hole capture, $\eta_{c,2}$) must also be energy sufficient to initiate the transfer of an electron from the neutral polymeric species to the oxidized NC. Figure 5c draws attention to the effect of driving force on photocurrent generation. Notice that PEDOT and ProDOT films display larger photocurrents compared to P(Et)$_2$ProDOT films at similar [P(n)]/[P(ox)] ratios (e.g., ca. 0.15), which is due to their increased driving force for hole capture at the more negative potentials needed to achieve these concentration ratios.

Photoelectrochemistry of CdSe NC-Sensitized Polymer Films: Effect of NC Diameter. We next varied the diameter of the tethered CdSe NC, using only one polymer host, and found changes in the onset potential for net cathodic photocurrent, and significant effects on IQE. A series of electrodeposited P(Et)$_2$ProDOT films were modified with CdSe NCs of 3.3, 5.0, or 7.0 nm diameter. Figure 6 shows FE-SEM data for these NC-modified P(Et)$_2$ProDOT films with estimated coverages of 32 ± 3, 64 ± 7, and 57 ± 7% EML, respectively. Figure 7a shows semilog $J_{ph}-V$ plots for three NC-sensitized P(Et)$_2$ProDOT films that vary only in the diameter of the tethered CdSe NC (see Supporting Information Figure S3 for the extracted dark and photocurrents). The normalized photocurrent action spectra (−0.15 V) were once again similar to the solution absorbance spectra (Figure 7b). IPCE values (−0.15 V, 500 ± 5 nm) were converted to relative IQE values, normalized to the highest IQE for 3.3 nm diameter NCs, and tabulated along with the measured onset potentials in Table 2.

Smaller CdSe NCs displayed a more positive onset potential for cathodic photocurrents (a ca. 50 meV shift for 3.3 nm versus 7.0 nm diameter NCs), as expected if the excess free energy for hole-capture from the photoexcited NC controls the overall reaction rate. [P(n)]/[P(ox)] in the polymer host film in this potential window (i.e., 0.15 to 0.11 V) changes by less than 5%; we therefore hypothesize that the change in the onset potential for the three polymers arises mainly from shifts in E_{VB} associated with changes in NC diameter.

Figure 8a shows a schematic energy level diagram highlighting the overall charge transfer processes near the onset potential. The positive shift in the onset potential is rationalized by taking into account a small negative shift (relative to the electrochemi-

(71) Dunphy, D. R.; Mendes, S. B.; Saavedra, S. S.; Armstrong, N. R. *Anal. Chem.* **1997**, *69*, 3086–3094.

Table 1. Measured Turn On Voltages, IPCE, NC Coverage (Γ), LHE, Relative Values of IQE, and [*P*(n)]/[*P*(ox)] for Poly(thiophene) Films with Tethered 5 nm Diameter CdSe NCs in the Presence of 5 mM MV^{+2}(aq)

polymer	turn on (V vs Ag/AgCl)	IPCE[a] (%)	Γ[b] % EML	LHE[c] (%)	IQE[d] (−0.15 V)	[n]/[ox][e] (−0.15 V)
P(Et)2ProDOT	0.13 ± 0.02	0.27 ± 0.01	64 ± 7	0.30 ± 0.03	1.0 ± 0.1	1.25 ± 0.05
PProDOT	0.10 ± 0.02	0.15 ± 0.01	59 ± 6	0.28 ± 0.03	0.6 ± 0.1	0.25 ± 0.03
PEDOT	0.05 ± 0.02	0.09 ± 0.01	63 ± 5	0.3 ± 0.02	0.5 ± 0.1	0.17 ± 0.02

[a] Incident photon to current efficiency (IPCE) measured with 500 nm light at −0.15 V. [b] Surface coverage (effective monolayer, EML) estimated from FE-SEM images. [c] Light harvesting efficiency (LHE) calculated using measured coverage and estimated extinction coefficient at 500 nm. See Figure S1 in Supporting Information for estimated extinction spectra. [d] Internal quantum efficiency (IQE) at 500 nm, normalized the highest IQE seen, for CdSe NCs captured on $P(Et)_2$ProDOT films. [e] [*P*(n)]/[*P*(ox)] measured at −0.15 V using data similar to Figure 4b.

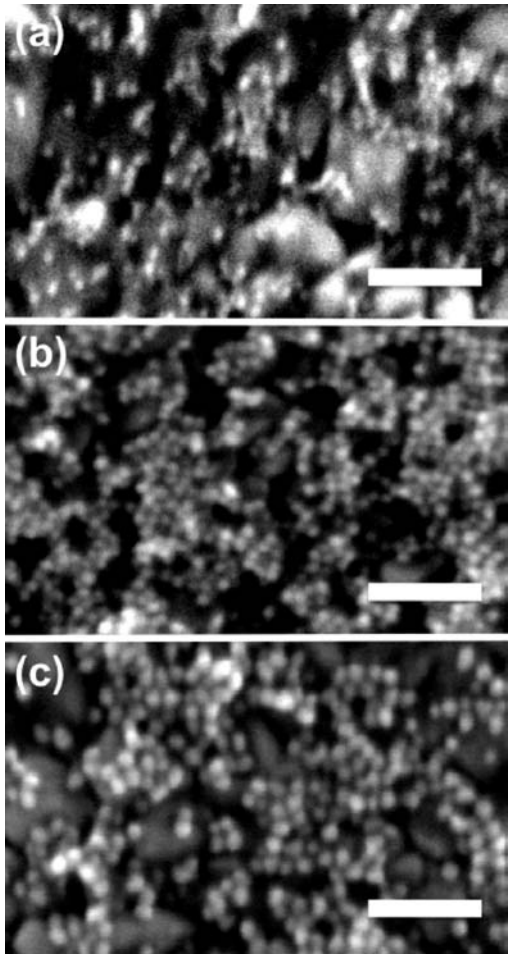

Figure 6. Plane-view FE-SEM images of $P(Et)_2$ProDOT polymer sensitized with (a) 3.3 nm, (b) 5.0 nm, and (c) 7.0 nm diameter ProDOT-CA-capped CdSe NCs via electrochemical cross-linking. The scale bar in each image is 50 nm.

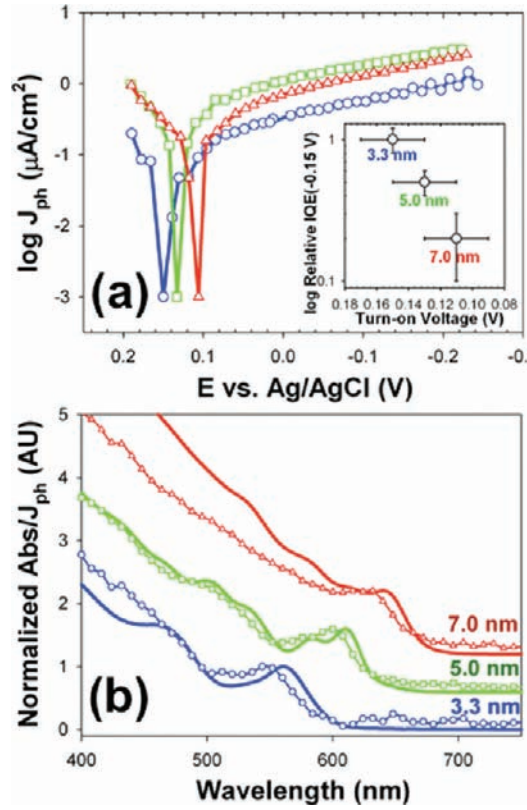

Figure 7. (a) Semilog photocurrent (J_{ph}) vs potential plots for $P(Et)_2$ProDOT films sensitized with 3.3 nm (blue circles/line), 5.0 nm (green squares/line), and 7.0 nm (blue triangles/line) CdSe NCs in the presence of MV^{+2} (5 mM in aqueous 0.1 M $LiClO_4$). Excitation was performed with 500 ± 5 nm radiation (2.1 mW cm^{-2}) using a band-pass-filtered Xe arc lamp. (b) Photocurrent action spectra at −0.15 V (symbols/lines) and solution absorbance spectra (lines) are similar, implying that the CdSe NCs are responsible for the generation of photocurrents (the spectra are stacked for clarity). The inset in part a displays a logarithmic relationship between the relative IQE and turn on voltage, implying a Marcus-like relationship is responsible for the observed NC size-dependent trends.

cal scale) in E_{VB} for the CdSe NCs with increasing diameter, where an overpotential (η_c, see also Figure 5) must be overcome before the rate of hole capture competes successfully with the back electron transfer reactions discussed above, hence the differences in onset potentials for the three different NC diameters. Assuming that electron capture by MV^{+2} is fast regardless of E_{CB} for the NC, a decrease in onset voltage is expected, and observed, as NC diameter decreases.[44]

The effective mass approximation (EMA, excluding polarization effects) predicts that E_{VB} should shift on the order of ca. 90 mV proceeding from 3.3 to 7.0 nm diameter NCs, close to earlier predictions by Brus,[44] and our photoelectrochemical data shown here. This EMA is based on the larger effective hole mass ($m_h = 1.14m_o$) of CdSe NCs relative to that of the effective electron mass ($m_e = 0.13m_o$),[72] where m_o is the free electron mass ($m_o = 9.11 \times 10^{-31}$ kg) (i.e., most of the shift in the band gap observed in the absorption spectra of these NCs is attributed to shifts in E_{CB}).[20] Earlier UV-photoemission (UPS) studies of ionization potentials of CdS NC monolayer on Au also demonstrated small shifts in E_{VB} with changes in NC diameter in this same size range.[73] Electrochemical studies of the redox processes in ligand-capped CdSe NCs confirms the small shifts in E_{VB} seen in these other experiments as NC diameter is

(72) Norris, D. J.; Efros, A. L.; Rosen, M.; Bawendi, M. G. *Phys. Rev. B* **1996**, *53*, 16347–16354.
(73) Colvin, V. L.; Alivisatos, A. P.; Tobin, J. G. *Phys. Rev. Lett.* **1991**, *66*, 2786–2789.

Table 2. Onset Potentials, IPCE, Coverage, LHE, and IQE for a Series of CdSe NC-Sensitized $P(Et)_2$ProDOT Thin Films with Different NC Diameters in the Presence of 5 mM MV^{+2}(aq)

NC diameter (nm)	turn on (V vs Ag/Cl)	IPCE[a] (%)	Γ[b] % EML	LHE[c] (%)	IQE[d] (−0.15 V)
3.3	0.15 ± 0.02	0.09 ± 0.01	32 ± 5	0.05 ± 0.01	1.0 ± 0.2
5.0	0.13 ± 0.02	0.27 ± 0.01	64 ± 7	0.30 ± 0.03	0.5 ± 0.1
7.0	0.11 ± 0.02	0.2 ± 0.1	57 ± 7	0.7 ± 0.1	0.2 ± 0.1

[a] Incident photon to current efficiency (IPCE) measured with 500 nm excitation at −0.15 V. [b] Surface coverage (effective monolayer, EML) estimated from FE-SEM images. [c] Light harvesting efficiency (LHE) calculated using measured coverage and estimated extinction coefficient at 500 nm. See Figure S6 in Supporting Information for estimated extinction spectra. [d] Internal quantum efficiency (IQE) at 500 nm, normalized to the highest IQE (for 3.3 nm diameter NCs).

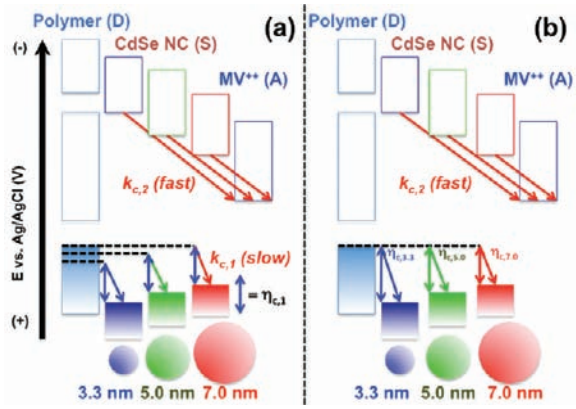

Figure 8. Schematic illustrations of the observed trends in (a) turn on voltage and (b) relative IQE at −0.15 V for $P(Et)_2$ProDOT polymer films sensitized with CdSe NCs of various diameter. (a) The negative shift in onset potential with increasing nanocrystal diameter is associated with a constant overpotential ($\eta_{c,1}$) for hole capture from the doped polymer for each nanocrystal. The increase in E_{VB} energy of the nanocrystal as a function of size necessitates increased negative overpotentials for the hole capture process to compete with back reactions. (b) The increase in relative IQE with decreasing nanocrystal diameter is due to an increase in the overpotential for hole capture for smaller nanocrystals relative to larger nanocrystals. The increased overpotential is associated with a Marcus-like exponential increase in the excess free energy for hole capture, and its associated rate.

varied.[74] Our own recent UPS studies of monolayer-tethered CdSe NCs confirm that shifts in E_{VB} as a function of NC diameter are smaller than 0.1 eV, i.e. most of the shift in energy with changing NC diameter is manifest in changes in E_{CB}.[45]

The relative IQE values (−0.15 V, 500 ± 5 nm), however, showed a strong dependence on NC diameter (Table 2). The 3.3 nm diameter CdSe NCs showed IQE values ≥5× those observed for 7 nm diameter NC. Figure 8b shows a schematic energy band diagram that summarizes the observed relative IQE trend versus NC diameter at −0.15 V, where an increased driving force for hole-capture, with decreasing NC diameter, is expected to lead to an exponential increase in the rate of charge transfer and net cathodic photocurrent. The inset of Figure 7a shows an exponential relationship between turn on voltage (E_{VB}) and IQE. As expected, smaller NCs provide a larger driving force for hole capture (η_c) from the polymer, associated with an increase in E_{VB}, leading to an increase in the rate of hole capture by the host polymer.

Conclusions

We have presented here an enabling methodology for attachment of functionalized semiconductor nanocrystals to electron-rich polymer hosts using potential step and pulsed-potential step electrodeposition protocols. Our electrodeposition approach provides for dense, highly electroactive polymer films which may find application in NC-sensitized photoelectrochemical energy conversion platforms, and as "hole-selective" contacts for photovoltaic devices.[3,48,49,58] Nanometer scale control over the placement of properly functionalized semiconductor nanocrystals has been demonstrated, providing for asymmetric attachment only at the polymer/solution interface, or homogeneously in the bulk of the polymer film.[47] This approach should provide for creation of polymer/nanocrystal composites (both semiconductor and oxide) in photovoltaic applications where hole transport and charge collection may be significantly enhanced.

The results presented here suggest that a highly doped conductive polymer can serve as an electron donor to photoexcited CdSe NCs, provided that [*P*(n)]/[*P*(ox)] is large enough to minimize back electron transfer reactions. Both the ease of reduction of the host polymer and the nanocrystal diameter (which controls E_{VB} and E_{CB}) affect the onset potential for cathodic photocurrent and photocurrent generation efficiency (IQE), parameters which are key in optimizing the energy conversion efficiency of photoelectrochemical and photovoltaic energy conversion systems.[21,22]

Some general design rules are apparent when designing these hybrid energy conversion materials: size and composition of semiconducting NCs must be considered in the context of frontier orbital energies (redox potentials for doping/dedoping) of the host polymer. In either type I or type II heterojunctions involving hole-transporting polymer hosts and NCs, smaller diameter NCs are predicted to lead to higher rates of charge transfer (hole capture) by the host polymer.[21,22] The larger band gaps and smaller relative absorption cross sections of smaller versus larger NCs, or different NCs with even lower E_{VB} energies (e.g., CdTe, PbSe, etc.), however, will require compromises in host polymer composition and energetics, and size of the NC when designing a PEC or PV cell based on NCs as the principal light absorbers.[19,21,22]

Achieving full rectification of the dark and photoelectrochemical activity (minimization or elimination of back reactions) would further greatly enhance the overall efficiency of these systems. Optimization of these materials must focus on (i) minimizing these back reactions, which is challenging when NC surface coverage at the polymer/solution interface is only ca. one equivalent monolayer, and (ii) increasing the active surface areas of the polymer host, thereby increasing optical densities of the NC-modified polymer, retaining vectorial electron transport.

An interesting question, not yet resolved, arises from the apparent difference in frontier orbital energies, E_{VB} and E_{CB}, measured in high vacuum environments (e.g., where they are determined from UV-photoemission experiments), and the inferred values of these energies derived from solution elec-

(74) Inamdar, S. N.; Ingole, P. P.; Haram, S. K. *ChemPhysChem* **2008**, *9*, 2574–2579.

trochemical experiments, where the NC is surrounded by a high dielectric constant solvent and supporting electrolyte. Thus far it is apparent that these energies, referenced to the vacuum scale, may be 0.5−0.8 eV smaller (closer to the vacuum level) in electrolytes versus those derived from high vacuum environments.[16,45,73,74] These are significant differences inasmuch as they limit our confidence in estimating the excess free energies available in electron transfer events to/from the NC, which control photoelectrochemical efficiencies (Figure 5a), electron transfer processes leading to light emission from the NC,[75−77] and their relative stabilities with respect to the host environment. The role that ligand-capping plays in determining E_{VB} and E_{CB} energies is also clearly important, and studies in progress focus on characterization of these energies as function of both capping ligand and host environment.[45]

Acknowledgment. The authors gratefully acknowledge the Division of Chemical Sciences, Geosciences, and Biosciences, Office of Basic Energy Sciences of the U.S. Department of Energy through Grant DE-FG03-02ER15753 for the majority of the personnel funding of this project, and grants from the National Science Foundation (CHE 0517963), the NSF Science and Technology Center for Materials and Devices for Information Technology Research (DMR-0120967), and the Arizona Board of Regents TRIF Program−Arizona Research Institute for Solar Energy (AzRISE) for support of the purchase of all of the equipment used in this work, and associated technologies relevant to the characterization of semiconductor nanoparticles, ultrathin polymer films, and the dynamics of photoinduced electron transfer. The authors also gratefully acknowledge the assistance of Dr. Erin Ratcliff in optimizing the electrodeposition protocols used in this work and the critical reading of this manuscript by Dr. Andrea Munro.

Supporting Information Available: Entire Experimental Section and detailed experimental procedures for determining LHE, IPCE, IQE, and the spectroelectrochemical and electrochemical properties of CdSe NC-sensitized polymer films. This material is available free of charge via the Internet at http://pubs.acs.org.

JA907782F

(75) Bae, Y.; Myung, N.; Bard, A. J. *Nano Lett.* **2004**, *4*, 1153–1161.
(76) Bard, A. J.; Ding, Z. F.; Myung, N. Electrochemistry and electrogenerated chemiluminescence of semiconductor nanocrystals in solutions and in films. In *Semiconductor Nanocrystals and Silicate Nanoparticles*; SPRINGER-VERLAG: BERLIN, 2005; Vol. 118, pp 1−57.
(77) Myung, N.; Ding, Z. F.; Bard, A. J. *Nano Lett.* **2002**, *2*, 1315–1319.